INTERNATIONAL JOURNAL OF NUMERICAL MODELLING: ELECTRONIC NETWORKS, DEVICES AND FIELDS
Int. J. Numer. Model. 2017; 30: e2129
Published online 18 December 2015 in Wiley Online Library (wileyonlinelibrary.com). DOI: 10.1002/jnm.2129

Knowledge based response correction method for design of reconfigurable N-shaped microstrip patch antenna using inverse ANNs

Ashrf Aoad[1,*,†], Murat Simsek[2] and Zafer Aydin[3]

[1]*Department of Electrical and Electronics Engineering, Bahcesehir University, Istanbul, Turkey*
[2]*Department of Astronautical Engineering, Istanbul Technical University, Istanbul, Turkey*
[3]*Department of Computer Engineering, Abdullah Gul University, Kayseri, Turkey*

SUMMARY

Artificial neural networks (ANNs) have been often used for engineering design problems. In this work, an inverse model of a reconfigurable N-shaped microstrip patch antenna which is formed by ANN is considered to find design parameters. For this task, knowledge-based response correction consists of two steps, which include generating response using multilayer perceptron as a first step and correcting this response using knowledge based methods such as source difference, prior knowledge input, and prior knowledge input with difference as a second step. The proposed antenna has four states of operation controlled by two Positive-Intrinsic-Negative (PIN) diodes with ON/OFF states. The two-step ANN models are inversely trained using the optimum of the resonant frequency parameter as the input and the physical dimensions of the proposed antenna as outputs of the multilayer perceptron. The outputs and, in some methods, the input parameters of the multilayer perceptron are sent as input to the knowledge-based models while the obtained outputs from the two steps are the results of the new physical dimensions of the redesigned reconfigurable antenna that will be compared and analyzed. This input/output complexity of the proposed reconfigurable antenna allows an accurate and fast inverse model to be developed with less training data. Users may use this antenna and its ANN models to develop new products in the market where any frequency in the operating region can be given to the input to result an appropriate form of the new reconfigurable antenna. Copyright © 2015 John Wiley & Sons, Ltd.

Received 9 March 2015; Revised 9 September 2015; Accepted 21 October 2015

KEY WORDS: inverse artificial neural network; knowledge based models; antenna design; reconfigurable microstrip antenna; PIN diodes

1. INTRODUCTION

With the fast development of wireless communication, especially in MIMO techniques [1], radar systems, mobile hotspots, and portable computers [2], the reconfigurable microstrip antennas are gaining great responsiveness; their behavior can be adapted with changing complex system requirements or environmental conditions, and they supply additional functionality for any wireless communication systems [3]. They can also operate in wider instantaneous frequency bandwidths, radiation patterns with more desirable side lobe distributions. In addition, they allow the reuse of resonant frequencies and increase the capacity of the communication systems [4]. Various reconfiguration techniques have been employed based on the integration of radio-frequency microelectromechanical systems, PIN diodes, varactors, and photoconductive elements [5, 6]. In this study, PIN diodes are employed for their low rate of loss and low cost [7]. The switching states that have been studied in this paper are OFF–OFF, ON–ON, and ON–OFF states. Each state possesses a wide range of frequencies that make

*Correspondence to: Ashrf Aoad, Department of Electrical and Electronics Engineering, Bahcesehir University, Istanbul, Turkey.
†E-mail: ashawad@hotmail.com

the use of the proposed reconfigurable N-shaped microstrip patch antenna (RNSMPA) more suitable for particular applications when compared with similar reconfigurable antennas with PIN diode studies in [4, 7–9]. Therefore, its performance makes it an ideal candidate for the wireless communication systems.

During the last decade, there has been a growing demand for applying optimization methods [10] to the antenna design, such as Bayesian algorithms [11], genetic algorithms [12], space mapping [13, 14], and ANNs [15, 16].These algorithms are used not only for the antenna design process, but also for fast operation simulations and improving the accuracy of the models [5]. ANNs are presented as an advantageous tool for RF/microwave modeling and design because of their mathematical simplicity. They have also been explored as a solution technique for design, optimization [17], and modeling to form linear–nonlinear input/output relationships from the corresponding data [5]. In certain cases, knowledge from modeled structures is available such as data from coarse models, equivalent models, semi-analytical equations, and computational and empirical formulas [18]. In knowledge based modeling, the existing knowledge is incorporated as input and/or output parameters of a learning model (e.g., an ANN) [19]. Knowledge-based modeling is more accurate, faster, has better extrapolation performance and requires less training data compared with the multilayer perceptron (MLP) [18]. In antenna design, typically, a forward ANN model is used where the physical dimensions are as input parameters and the *S*-parameters as outputs. However, in an inverse ANN knowledge-based model, the frequency points supplied as inputs and the physical dimensions as outputs [20–22].

This paper presents a novel solution by using a knowledge-based response correction inverse model of ANN for designing RNSMPA as an alternative to EM simulations. The design contains two steps: MLP followed by a knowledge-based model such as a source difference method (SD), prior knowledge input method (PKI) [18, 23] or prior knowledge input with difference method (PKI-D) [5, 19]. It is important to note that the outputs of MLP present a coarse information about the antenna, which is later corrected by the knowledge-based models. Finally, the parameters obtained from the ANNs are redesigned by the EM Computer Simulation Technology (CST) Studio and compared with the original (fine) model. The proposed solutions demonstrate to be particularly useful in situations where a resonant frequency is the only input used to result in various geometrical dimensions.

2. RECONFIGURABLE ANTENNA DESIGN

The PIN switch-based RNSMPA under researching is shown in Figure 1. Several challenges are addressed during the design phase, such as the system performance (bandwidth, wide range of operating frequency, directivity, etc.), antenna size, cost, profile, capable of fabrication, and ability to reconfigure from one state to the next [2].

The studied antenna presents a novel reconfigurable microstrip-patch antenna. This RNSMPA consists of three layers and a feeding system. The radiating conductors (first layer) consist of two-mirrored triangles as shown in Figure 1(a) where the dimension parameters of L_1, L_2, L_3, W_1, and W_4 set to 0.8 cm. They are modeled on an Flame Retardant, type 4 (FR-4) substrate board (second layer) with a thickness of 0.2 cm and a relative permittivity of 4.3. The ground plane (third layer) is printed on

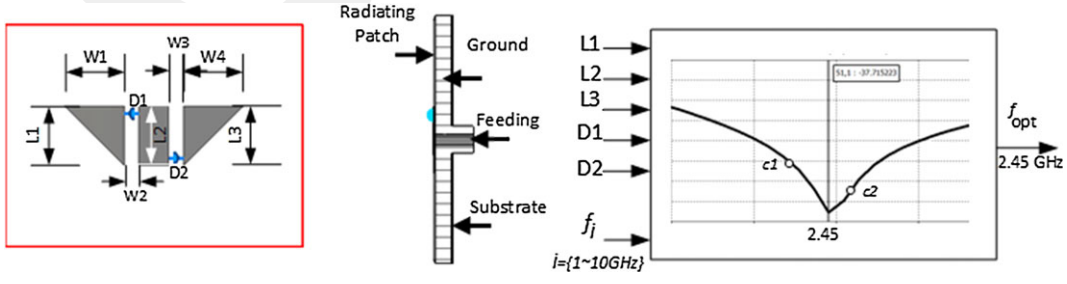

(a) (b) (c)

Figure 1. Reconfigurable antenna (a) top view, (b) side view, and (c) input/output relationship for electromagnetic simulator, where c_1 and c_2 represent closest points to the optimum frequency point.

DOI: 10.1002/jnm

the back side of the substrate [24]. The unfilled space (W_2 and W_3) between the triangles and the mid microstrip that includes two PIN diodes (D_1 and D_2) is 0.2 cm. The PIN diodes positioned in the upper left and lower right sides of the triangle patches distribute the current paths on the microstrips depending on its bias state [25]. When the switching diodes are open (OFF–OFF state), the current is distributed on the middle conducting patch only, and the RNSMPA operates in a lower frequency band (2 ~ 3.9 GHz). When both of the diode switches are closed (ON–ON state), the effective length of the RNSMPA becomes higher causing the antenna to operate in a mid-frequency band (4 ~ 6 GHz). If a diode is open while the other is closed (ON–OFF state), the RNSMPA operates in a higher frequency band (8 ~ 10 GHz) as the effective patches are the middle rectangle and the triangle that is connected to it. Therefore, the resonant frequencies are a function of the switch positions (i.e., the diode states) [15]. The feeding system is centered at the center of mid patch with a radius of 0.065 cm as shown in Figure 1(b). The optimum frequency and points that are close to it (i.e., c_1 and c_2 circles as shown in Figure 1(c)) are at the heart of the design process of this study. To realize the ON and OFF states, two different resistors are used for the PIN diodes [26]. The large resistor has a resistance value of 130 Ohms to enable the locking of the direct current on the surface of the triangle patches when used in the OFF state, which is considered a reverse biased and almost represented as an open circuit [4]. The small forward resistor has a value of 5 Ohms when used in the ON state and almost represented as a short circuit [4]. For simplicity, the series inductor and parallel capacitor of the lumped elements are neglected in the equivalent circuit model [8, 26]. In order to perform this nonlinear function, minimum and maximum of the generated training data is tabulated in Table I. Other parameters that are shown in Figure 1, but not shown in Table I such as the width of triangles (W_1 and W_4), the radius of the feeding, unfilled spaces (W_2 and W_3), thickness of radiating patch, ground plane, and substrate, are not considered in training data.

3. PROPOSED KNOWLEDGE-BASED RESPONSE CORRECTION METHOD

This section describes the knowledge-based response correction method (KBRC) where existing knowledge (frequency data set) is combined with neural networks as shown in Figure 2. Various effects of adding knowledge/information on the performance of ANN models are noticed, such as generalization ability, extrapolation ability, and model reliability [18]. In KBRC modeling, existing coarse model (MLP model's output) is used to construct input/output relationships of the component model. The proposed KBRC inverse model consists of a two-step neural network followed by EM simulator to

Table I. Representative values of the minimum, maximum, and number of samples of the lengths and resistance parameters.

Parameters	Symbol	Minimum	Maximum	Samples
Length of the left patch	L_1 (cm)	0.8	2	9
Length of the mid patch	L_2 (cm)	0.7	2	9
Length of the right patch	L_3 (cm)	0.65	2	9
ON state (D_1 or D_2)	R_{ON} (Ω)	5	—	1
OFF state (D_1 or D_2)	R_{OFF} (Ω)	—	130	1
Frequency	f_i (GHz)	1	10	100

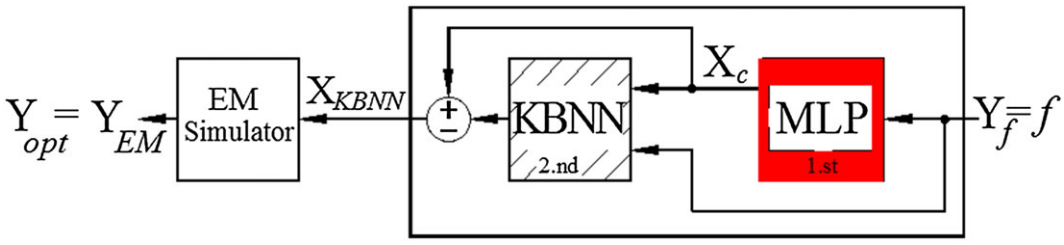

Figure 2. General electromagnetic (EM)-knowledge-based response correction (KBRC) inverse model.

DOI: 10.1002/jnm

redesign the output of X_{KBNN} for obtaining corrected response of the RNSMPA, which is represented by Y_{EM}. Thus, the relationship between the inputs of Y and the outputs of X is multidimensional and nonlinear [27]. Input for the EM-KBRC inverse models is mainly the frequency information only (f_f) of the fine model, while outputs are the desired physical parameters of the reconfigurable antenna.

In order to train the EM- KBRC inverse models, a number of EM, MLP, and knowledge-based neural network (KBNN) simulations need to be implemented. These simulations are necessary because it is important to display input/output relationships through EM-KBRC inverse model. The model proposed in Figure 2 can process nonlinear and multiple input/output variables effectively [28], providing good results for Y_{EM} ($Y_{EM}=f_{opt}=Y_{f-MLP}$, Y_{f-SD}, Y_{f-PKI}, and Y_{f-PKID}).

The training data obtained from the EM simulator has 72,900 samples, which are computed according to Table I by considering all possible combinations as $100\times9\times9\times9\times1\times1=72{,}900$ [15]. This large amount of training data is reduced to 86 samples only. The reduction procedure depends on the selection of optimum points for resonant frequencies, which are located by the lower value of the return loss [29]. For covering a wide range of resonant frequencies, which are spanned from 2 to 10 GHz (excluding the interval from 6.1 to 7.9 GHz) with a step size around 100 MHz between the successive frequency points. Some frequency points are selected to be close to the optimum frequency points as shown in Figure 1(c).

In the models testing stage, a new testing data set of input/output samples selected inside the training data is used to test the accuracy of the models for interpolation [27]. In addition, selecting a point of an input sample outside the training data is for extrapolation [19].

3.1. Multilayer perceptron

Multilayer perceptron [5, 13, 23] (without any knowledge based) consists of three perceptron layers lined as an input layer (Y), one or more hidden layers, and finally, an output layer (X). Each layer contains a number of neurons, which can be denoted as processing elements. There are interconnections between neurons as well. Every interconnection has a weight parameter linked to it, which are learned from the available training data. Each neuron receives data from the neighboring neurons at the previous layer and computes a weighted sum, which passes through an activation function to produce an output for that neuron [5]. The function of the input and the output vectors can be presented as $X=f(Y)$. In this study, the input is $Y_f=[f]^T$, and the predicted output is $X_C=[L_1, L_2, L_3, D_1, D_2,]^T$. D_1 and D_2, reflect the state of the diodes (the same procedure is applied on the following methods).

The EM-KBRC inverse models that will follow, MLP is the first step in which its output is considered as a coarse model (X_C) as shown in Figure 3.

Equations (1) and (2) represent the training error (e) for ith iteration and f_{opt} which gives frequency at minimum of Y_{f-MLP}, respectively. Training process updates weighting coefficients of MLP until stopping criteria is satisfied. Equations (1) and (2) are same as a general principle in the next methods.

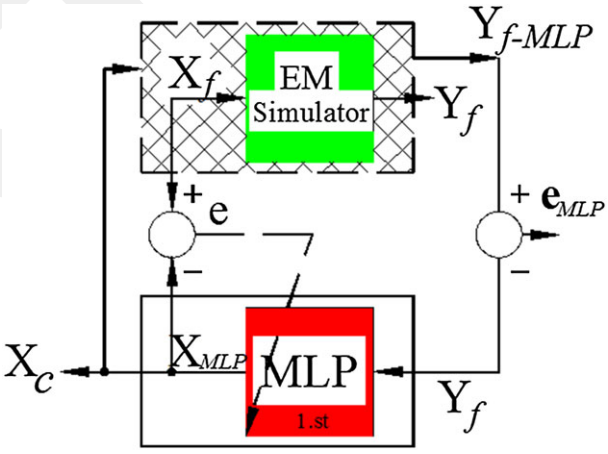

Figure 3. First step of electromagnetic (EM)-multilayer perceptron inverse model.

DOI: 10.1002/jnm

$$e^i = X_f^i - X_{MLP}^i. \tag{1}$$

$$f_{opt} = \underset{f}{\arg\min} \left\{ Y_{f-MLP} \right\}. \tag{2}$$

3.2. Source difference method

The SD method [5, 18, 23] combines two training data sets to be the target of the network, which are the EM simulation output $X_f = [L_1, L_2, L_3, D_1, D_2,]^T$ representing the fine data and the output response of MLP (X_C) obtained from the first step as shown in Figure 4. Thus, the input parameter of the SD (hatched MLP box) is only $Y_f = [f]^T$, the predicted output $X_{SD} = X_C + X_{MLP}$, while the target is $\Delta X_{SD} = X_f - X_C$ as shown in Figure 4.

The function of the input and the output of the redesign phase of EM simulation is presented as follows:

$$Y_{f-SD} = g_{EM}(X_{SD}), \tag{3}$$

where Y_{f-SD} is the optimum resonant frequency (f_{opt}) that is obtained by redesigning predicted output of the second step (X_{SD}). e_{SD} is the error measure computed as the absolute difference between f_{opt} and Y_f, which can be calculated by the following equation:

$$e_{SD} = \left| f_{opt} - Y_f \right| \tag{4}$$

Equations (3) and (4) are same as a general principle in all methods.

3.3. Prior knowledge input method

The PKI was proposed in [5, 18, 23]. In this method, the output response of MLP (X_C) is used as extra input for PKI (hatched MLP box) in addition to the original fine model response (Y_f). The target response of PKI is the fine model input parameters (Y_f). Therefore, the input/output mapping is constructed between the output response of MLP (X_C) besides the fine model response (Y_f) and the target response (X_f). Thus, the input parameter for PKI is $Y_{PKI} = [L_1, L_2, L_3, D_1, D_2,]^T$ as shown in Figure 5.

3.4. Prior knowledge input with difference method

The PKI-D was proposed in [5, 19]. It exploits the advantages of two knowledge-based methods, which are explained previously (PKI and SD). The output response of MLP (X_C) and the fine model response (Y_f) are utilized as the inputs of PKI-D (hatched MLP box). The difference between fine model input parameters (X_f) and the output response of MLP (X_C) is utilized as the output of PKI-D. Therefore, the input parameter is $Y_{PKID} = [L_1, L_2, L_3, D_1, D_2, X_C]^T$, while the target is $\Delta X_{PKID} = X_f - X_C$ as shown in Figure 6.

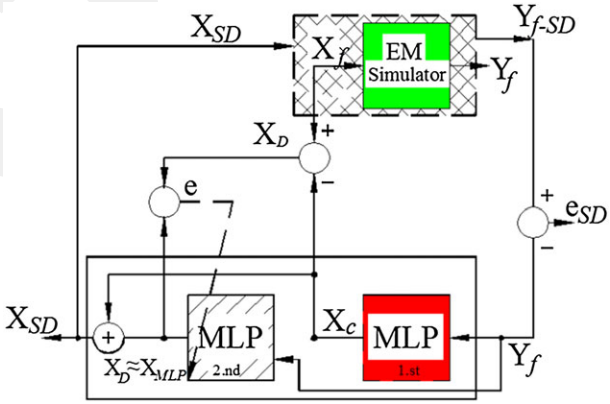

Figure 4. Two steps of electromagnetic (EM)-knowledge-based response correction (KBRC) inverse model for source of difference.

DOI: 10.1002/jnm

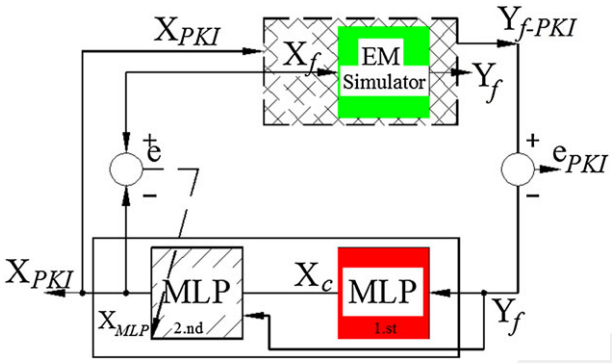

Figure 5. Two steps of electromagnetic (EM)-knowledge-based response correction (KBRC) inverse model for prior knowledge input.

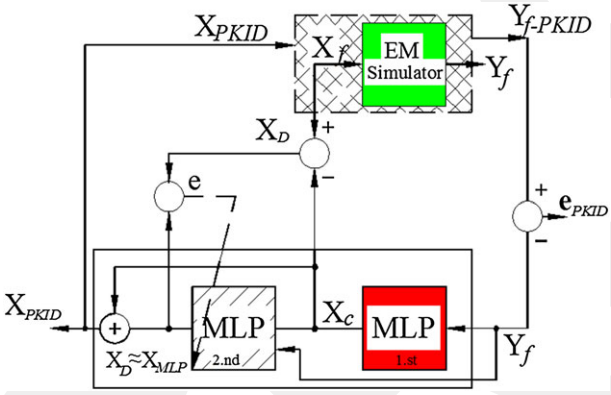

Figure 6. Two steps of electromagnetic (EM)-knowledge-based response correction (KBRC) inverse model for prior knowledge input with difference.

4. TRAINING AND TESTING OF KNOWLEDGE-BASED RESPONSE CORRECTION INVERSE MODEL

There are three data sets that are considered to demonstrate the performance of KBRC method. A training data set includes the optimum and closest points for the resonant frequencies. Three optimum frequency points and corresponding three geometries are selected inside the training data set to show the test performance. Two more frequency points, which are not included by training data set, are selected as extrapolation points to check the performance of generalization capability of the proposed method as well. In the case of increasing the testing errors, the training process will be stopped for canceling overfitting of the training data [28]. Another important problem with ANN modeling is to determine the network architecture, which starts with a simple network, usually includes only one hidden layer with some neurons. By following the learning process, it is easy to note the accuracy and the speed achieved or not. If not, additional neurons are added to the hidden layer. Till identifying the optimal network architecture, adding neurons and layers will be continued. At the end of this procedure, the number of hidden layers is found to be two for all models. However, the number of neurons is in range (30–60) for MLP and (40–30) for KBNNs. ANN models are trained by using Levenberg–Marguardt algorithm [30, 31] with tangent-sigmoid transfer functions in the hidden layers and a purely linear function in the output layer. The training of the model is achieved by setting the learning rate (η) to 0.1 for MLP and 0.05 for KBNNs, the performance goal to 0.000001 for MLP and KBNNs and momentum coefficient (μ) to 0.02 for MLP and 0.1 for others. The regularization coefficient of the network is chosen as 0.2 where an L2-norm regularizer is used [31]. The normalized mean absolute error (NMAE) measure computes the absolute difference between the fine outputs and the outputs of ANNs and is used to assess the accuracy of the neural networks. NMAE is quantified as follows:

DOI: 10.1002/jnm

$$\mathrm{NMAE} = \sum_{j=1}^{N} \left(\frac{|Y_{fj} - t_j|}{|y_{fj}|} \right), \tag{5}$$

where the Y_{fj} represents the optimum value of the output of the fine model, t_j is the optimum value of ANNs output, and N is the number of the data samples in the test set. The whole ANN structures for both inverse MLP and knowledge-based methods, which are used for response correction, are realized by MATLAB ANN toolbox.

5. RESULTS AND DISCUSSION

The neural network models are repeatedly trained 50 times, and the physical dimensions of the RNSMPA are computed on the test sets to investigate the statistical behavior of the randomized network initialization. The accuracy of the models is presented by the average error and *S*-parameter curves, which are the results of re-simulating the physical parameters obtained from KBRC inverse models. The overall tendency is that KBNNs (hatched MLP in the figures) are trained by (40–30) neurons for two hidden layers in the second step, while MLP is trained by (30–60) neurons in the first step.

5.1. Interpolation results

Three sets of testing samples were selected inside training data. Each set presents a state of switching PIN diodes. Therefore, the results shown in Tables II, III, and IV of the physical dimensions of the proposed reconfigurable antenna present OFF–OFF, ON–ON, and ON–OFF states, respectively. Each method has various values for each input variable, where every method operates successfully at different resonant frequency bands. On the other hand, the physical parameters obtained from ANN inverse models were redesigned by the EM simulator and compared with the fine results as shown in Figures 7, 8, and 9, respectively. It is important to note that MLP results obtained by the first step of the EM-KBRC inverse models are not immediately corrected. However, SD, PKI, and PKI-D models in the

Table II. A comparison between the results obtained by ANN inverse models and EM model in OFF–OFF state.

Parameters	EM	MLP	SD	PKI	PKI-D
L_1 (cm)	0.8625	0.9103	0.8554	0.8766	0.9072
L_2 (cm)	1.25	1.6350	1.4392	1.4298	1.6236
L_3 (cm)	0.65	1.2818	0.9035	0.9073	1.1274
D_1 (Ω)	130	128.8989	128.0052	129.7975	130.3918
D_2 (Ω)	130	127.9286	130.2623	129.2136	131.7255
f_{opt} (GHz)	2.45	2.3636	2.4545	2.4545	2.4545
RL (dB)	−57.57	−35.76	−33.36	−38.47	−41.88

The results shown are the physical antenna parameters, optimum frequency point (f_{opt}), and return loss (RL).
ANN, artificial neural network; EM, electromagnetic; MLP, multilayer preceptron; SD, source of difference; PKI, prior knowledge input; PKI-D, prior knowledge input with difference.

Table III. A comparison between the results obtained by ANN inverse models and EM model in ON–ON state.

Parameters	EM	MLP	SD	PKI	PKI-D
L_1 (cm)	0.8625	1.0399	1.1114	1.0222	1.0017
L_2 (cm)	1.85	1.5279	1.5503	1.6146	1.6236
L_3 (cm)	0.9875	0.8254	0.8030	0.8661	0.9460
D_1 (Ω)	5	4.9996	3.8894	4.0437	2.7967
D_2 (Ω)	5	5.4031	4.1598	7.1811	3.3908
f_{opt} (GHz)	4.27	4.4545	4.3636	4.3636	4.3636
RL (dB)	−47.76	−29.16	−24.74	−26.19	−22.06

The results shown are the physical antenna parameters, optimum frequency point (f_{opt}), and return loss (RL).
ANN, artificial neural network; EM, electromagnetic; MLP, multilayer preceptron; SD, source of difference; PKI, prior knowledge input; PKI-D, prior knowledge input with difference.

DOI: 10.1002/jnm

Table IV. A comparison between the results obtained by ANN inverse models and EM model in ON–OFF state.

Parameters	EM	MLP	SD	PKI	PKI-D
L_1 (cm)	1.8375	1.8871	1.8634	1.8854	1.8690
L_2 (cm)	0.8	1.5342	1.2353	1.2295	1.1636
L_3 (cm)	0.65	0.9272	0.7786	0.8336	0.6618
$D_1(\Omega)$	5	3.4782	5.1865	4.8213	4.9795
D_2 (Ω)	130	130.1626	129.3746	128.5880	128.7705
f_{opt} (GHz)	8.60	8.3636	8.6364	8.5455	8.7273
RL (dB)	−10.92	−10.61	−10.93	−10.91	−10.75

The results shown are the physical antenna parameters, optimum frequency point (f_{opt}), and return loss (RL).
ANN, artificial neural network; EM, electromagnetic; MLP, multilayer preceptron; SD, source of difference; PKI, prior knowledge input; PKI-D, prior knowledge input with difference.

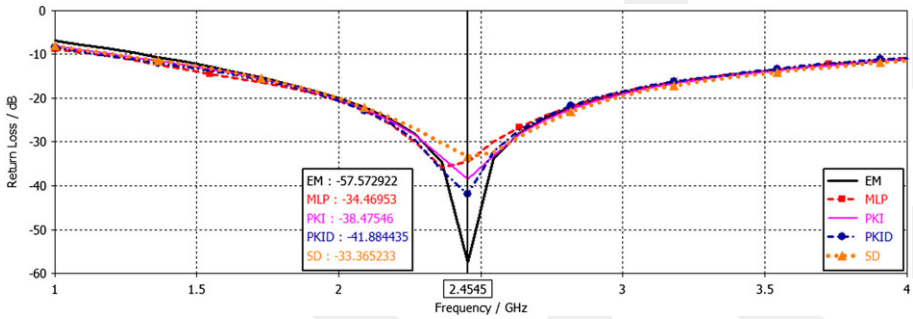

Figure 7. Model accuracy comparison of *S*-parameters for the redesigned artificial neural networks inverse models with the fine model when they are tested by internal testing data samples in OFF–OFF state.

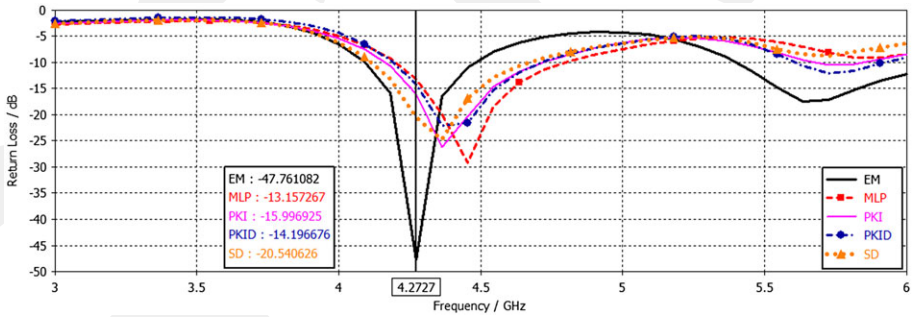

Figure 8. Model accuracy comparison of *S*-parameters for the redesigned artificial neural networks inverse models with the fine model when they are tested by internal testing data samples in ON–ON state.

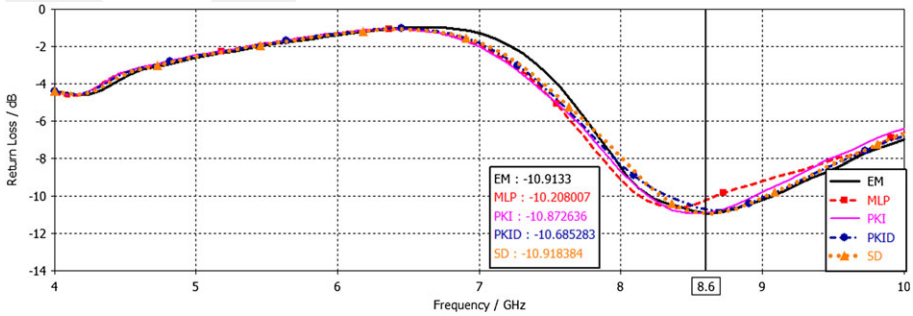

Figure 9. Model accuracy comparison of *S*-parameters for the redesigned artificial neural networks inverse models with the fine model when they are tested by internal testing data samples in ON–OFF state.

DOI: 10.1002/jnm

second step correct the results outputted by MLP in the first step. Either exact or closer to the optimum point of the resonant frequency of the fine (EM) model with different values for return loss are noticed. The fine (EM) model parameters in OFF–OFF state are shown in Table II.

Although the optimum resonant frequency matched exactly in PKI-D, PKI, and SD models, but differed in the form of the antenna. This difference depends on the obtained physical parameters. Table V shows the NMAE results for all models when the switching state of the PIN diodes is set to OFF–OFF, ON–ON, and ON–OFF, respectively. For all models, the NMAE is computed for the optimum points of the frequency. The NMAE of the frequency indicates that the optimum points of PKI, PKI-D, and SD match exactly in the value with the interpolation test frequency points (2.45 GHz for OFF–OFF state and 4.27 GHz for ON–ON state). However, left displacement is noticed for the optimum frequency point that is obtained by MLP at 2.36 GHz in OFF–OFF state as shown in Figure 7, and right displacement is also noticed for the MLP output at 4.45 GHz in ON–ON state as shown in Figure 8. According to NMAE rates of the frequency, the accuracy of the prior knowledge-based models is better than MLP. Moreover, Figure 7 shows that the optimum point of the frequency is 2.45 GHz for the fine, PKI-D, PKI, and SD models, but it is 2.36 GHz for MLP. For a target of return loss of $S_{11} \leq -10$ dB, the bandwidth is approximately 2.75 GHz.

The second testing data set is used for the ON–ON state. The evaluation of the results obtained in this state is similar to the OFF–OFF state.

Furthermore, the bandwidth of ANN inverse models is wider than that of the fine model. For a target of return loss of $S_{11} \leq -10$ dB, the bandwidth is around 0.65 GHz for ANN inverse models, while it is 0.38 GHz for the fine model. In addition f_{opt} has a deeper return loss value compared with ANN models.

In ON–OFF state, the evaluation of the results is not different from the previous states, where KBNN models still occupied the first accuracy rankings followed by MLP.

Table V demonstrates the NMAE results for the optimum points of the frequency (8.60 GHz) and return loss (−10.92 dB) when the PIN diodes are set to the ON–OFF state. The best match is achieved by KBNN models, SD followed by PKI and PKI-D models, while the MLP model is the worst model compared with the others. From Figure 9, it is clearly shown that all *S*-parameter curves of ANNs travels from 6.4 GHz to 7.85 GHz under the fine curve. However, the curve of MLP is above the other lines at 8.36 GHz and −11.61 dB to catches up again at 9.62 GHz and −10.92 dB. It is still the farthest curve from the optimum frequency and return loss values of the fine model.

Therefore, the wider bandwidth is noticed at the fine and KBNN models, which is around 0.8 GHz, while it is around 0.4 GHz for MLP model at a return loss of $S_{11} \leq -10$ dB.

From the results presented previously, it is noticed that KBNN models are more reliable and accurate than MLP models in the interpolation region. The antenna can be reconfigured to obtain new results as well.

5.2. Extrapolation results

The results given previously were trained on the test sets selected inside the training data set for interpolation [19]. In this section, results for external frequency samples are presented. Two external frequency samples were selected to test the ANN models and to find the switching state: 2.5 GHz and 5.7 GHz. It is important to notice that they are selected in order to test two regions of the frequency band (Section 2).

Table V. Model accuracy comparison of NMAE values of the optimum points of the frequency for the ANN models in all states.

State	Frequency (GHz)	MLP	SD	PKI	PKI-D
OFF–OFF	2.45	0.0353	0.0018	0.0018	0.0018
ON–ON	4.27	0.0432	0.0219	0.0219	0.0219
ON–OFF	8.60	0.0275	0.0042	0.0063	0.0148

NMAE, normalized mean absolute error; ANN, artificial neural network; MLP, multilayer preceptron; SD, source of difference; PKI, prior knowledge input; PKI-D, prior knowledge input with difference.

DOI: 10.1002/jnm

Tables VI and VII show that each method has various values for each input variable. In addition to that, every method operates successfully at different resonant frequencies when only a frequency sample used for testing the training data. Furthermore, the geometrical parameters obtained from ANN inverse models were redesigned by EM simulator to give new results as shown in Figures 10 and 11. The obtained values for D_1 and D_2 show that the switching state of the PIN diodes was OFF–OFF and ON–ON for external testing data samples of 2.5 GHz and 5.7 GHz, respectively. Note that there is no fine model in the extrapolation region that can be used for comparison.

The optimum values of the ANNs outputs are close to the external testing data sample of 2.5 GHz, which is defined by the axis maker in the following figures. It exactly occurs in the middle between the KBNN and MLP results as shown in Figure 10. This explains why the values of NMAEs are equal to

Table VI. A comparison between the results obtained by ANN inverse models with an external testing data sample of 2.5 GHz. The results shown are the physical antenna parameters, optimum frequency point (f_{opt}) and return loss (RL).

Parameters	External	MLP	SD	PKI	PKI-D
D_1 (cm)	—	0.8653	0.8083	0.8366	0.8925
L_2 (cm)	—	1.5871	1.3770	1.6395	1.4334
L_3 (cm)	—	1.1024	0.6788	1.0694	0.8655
D_1(Ω)	—	129.8831	128.4598	131.6531	129.9624
D_2 (Ω)	—	127.7753	130.0089	128.5265	130.8663
f_{opt} (GHz)	2.5	2.5455	2.4545	2.4545	2.4545
RL (dB)	—	−30.27	−48.97	−37.66	−40.12

ANN, artificial neural networks; MLP, multilayer preceptron; SD, source of difference; PKI, prior knowledge input; PKI-D, prior knowledge input with difference.

Table VII. A comparison between the results obtained by ANN inverse models with an external testing data sample of 5.7 GHz. The results shown are the physical antenna parameters, optimum frequency point (f_{opt}) and return loss (RL).

Parameters	External	MLP	SD	PKI	PKI-D
L_1 (cm)	—	0.7992	0.7620	0.7689	0.8177
L_2 (cm)	—	1.8813	2.0200	1.8955	2.0573
L_3 (cm)	—	1.6943	1.7955	1.6351	1.7543
D_1 (Ω)	—	6.7048	5.7839	5.2753	3.6356
D_2 (Ω)	—	6.0619	5.7485	5.4547	2.2511
f_{opt} (GHz)	5.7	5.8182	5.7273	5.8182	5.6364
RL (dB)	—	−18.80	−21.70	−20.02	−26.42

ANN, artificial neural networks; MLP, multilayer preceptron; SD, source of difference; PKI, prior knowledge input; PKI-D, prior knowledge input with difference.

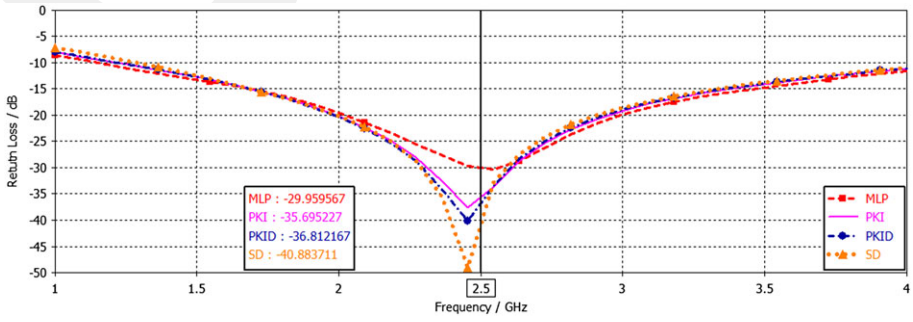

Figure 10. Model accuracy comparison of *S*-parameters for the redesigned artificial neural networks inverse models when they are tested by an external frequency sample of 2.5 GHz.

DOI: 10.1002/jnm

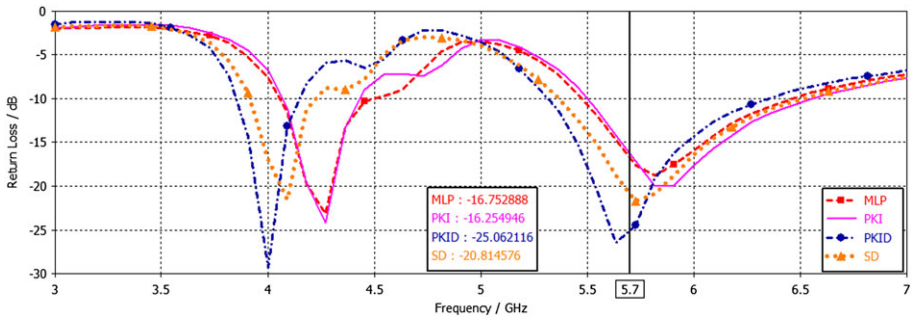

Figure 11. Model accuracy comparison of *S*-parameters for the redesigned artificial neural networks inverse models when they are tested by an external frequency point of 5.7 GHz.

each other as shown in Table VIII. This means that the output of MLP in the first step is displaced to the right side of the axis maker and KBNN's is displaced to the left side by equal amounts. In addition to the advantages mentioned previously, the bandwidth is around 2.8 GHz at a return loss of $S_{11} \leq -10$ dB for all models. The values of the return loss that are shown on the left of Figure 10 are the intersection points on the axis maker at 2.5 GHz. In addition to the intersected points of the return loss on the axis maker show the KBNN models have deeper values than MLP. The optimum points of the return loss are shown in Table VI.

Figure 11 shows that the redesigned reconfigurable antenna with new geometrical dimensions obtained by ANNs can operate over two resonant frequencies. Notice that both resonant frequencies operate in the ON–ON region.

The NMAE of the frequency for ANN models differs from one state to the next. SD is the closer to axis maker at 5.7 GHz then comes PKI-D followed by PKI and, lastly, MLP. KBNN models have deeper return losses as compared with MLP.

Tables IX and X show that either interpolation or extrapolation testing data sets can obtain excellent results. Specifically, PKI-D and SD methods have lower the return loss values at the optimum points of the frequency as shown in previous figures. Because the operating region under −10 dB is wide and

Table VIII. Model accuracy comparison of NMAE values between the ANN models optimum points of the frequency and the external frequency points.

Frequency (GHz)	NMAE			
	MLP	SD	PKI	PKI-D
2.5	0.0182	0.0182	0.0182	0.0182
5.7	0.0207	0.0048	0.0207	0.0112

NMAE, normalized mean absolute error; MLP, multilayer preceptron; SD, source of difference; PKI, prior knowledge input; PKI-D, prior knowledge input with difference.

Table IX. A comparison between the return loss results at the optimum points of the frequency in all states for interpolation.

Frequency (GHz)	Return loss (dB)				
	EM	MLP	SD	PKI	PKI-D
2.45	−57.57	−34.46	−33.36	−38.47	−41.88*
4.27	−47.76	−13.15	−20.54*	−15.99	−14.19
8.60	−10.91	−10.20	−10.91*	−10.87	−10.68

EM, electromagnetic; MLP, multilayer preceptron; SD, source of difference; PKI, prior knowledge input; PKI-D, prior knowledge input with difference.
*The lower value of return loss.

DOI: 10.1002/jnm

Table X. A comparison between the return loss results at the optimum points of the frequency for extrapolation.

Frequency (GHz)	Return loss (dB)				
	EM	MLP	SD	PKI	PKI-D
2.5	—	−29.95	−40.88*	−35.69	−36.81
5.7	—	−16.75	−20.81	−16.25	−25.06*

EM, electromagnetic; MLP, multilayer preceptron; SD, source of difference; PKI, prior knowledge input; PKI-D, prior knowledge input with difference.
*The lower value of return loss.

each method has different geometrical parameters, users can use them to design new reconfigurable antennas.

Curve models and tables are used in this study to depict the optimized physical structures of a reconfigurable antenna as shown in the cases presented. These cases lead to an optimal reconfigurable antenna under the conditions elaborated. Results show the advantages of ANN inverse models over the reconfigurable antennas as follows: (i) Number of neurons used in the hidden layers of KBNN is lower than MLP; (ii) the output of MLP (coarse model) can be corrected through KBNNs in most cases to be closer to the fine model; (iii) interpolation and extrapolation testing sets can be used to find an accurate model; (iv) less training data is applicable; (v) return loss is lower than −10 dB with voltage standing wave ratio less than 2 (Constatine, 2005), (vi) operating at different frequency bands with wide bandwidths and (vii) switching capability. (viii) The obtained values of the physical dimensions by inverse ANNs increased or decreased in most models from 20% to 40% compared with the original physical dimensions of the fine model; while to reach to this result by EM simulation design only, it will be needed to apply trial-and-error method (Khan & De, Design of Circular/Triangular Patch Microstrip Antennas using a Single Neutral Model, 2011), which often takes more time to get an exact or approximate result.

6. CONCLUSION

A KBRC method has been proposed that combines reconfigurable antenna with the power of learning from ANN inverse models. A detailed study about different states of the reconfigurable antenna is presented. A comparison between the different ANN methods used to redesign the state of the antenna is also presented. A new structure for ANNs is developed. This structure consists of two steps, MLP in the first step followed by KBNNs in the second step. The frequency of the fine model is the input for the MLP then the results obtained from the first step is corrected by passing through KBNNs in the second step to set out the physical dimensions of the reconfigurable antenna. These dimensions will be again redesigned by EM simulator to realize a new form of the reconfigurable antenna. Interpolation and extrapolation testing data sets were used to test neural network models for various PIN diode states. It is found that less training data is sufficient in KBRC method. The incorporation of such knowledge into ANNs is very useful to yield a reliable model when less training data is used. The achievement of such a low error indicates that trained models are accurate for designing reconfigurable antennas. In all states, KBNNs outperform MLP in the accuracy measures. The proposed reconfigurable antenna provides a wide operating range of resonant frequencies such as from 2 ~ 3.9 GHz in OFF–OFF state, from 4 ~ 6 GHz in ON–ON state and from 8 to10 GHz in ON–OFF state. Finally, this study may be introduced as a handy tool for marketing the reconfigurable antenna where the designer gives the required frequency of operation as input, and the KBRC method will give the geometrical dimensions of the reconfigurable antenna.

REFERENCES

1. Zhou Y, Adve RS, Hum SV. Design and Evaluation of Pattern Reconfigurable Antennas for MIMO Applications. *IEEE Trans Antennas Propag* 2014; **62**(3): 1084–1092.
2. Al-Zayed AS, Kourah MA, Mahmoud SF. Frequency-Reconfigurable Single- and Dual-Band Designs of a Multi-mode Microstrip Antenna. *IET Microwaves Antennas Propag* 2014; **8**(13):1105–1112.
3. Kumar S, Chamberland J-F, Huff GH. Reconfigurable Antennas, Preemptive Switching and Virtual Channel Management. *IEEE Trans Commun* 2014; **86**(4):1272–1282.

DOI: 10.1002/jnm

4. Song T, Lee Y, Ga D, Choi J. A Polarization Reconfigurable Microstrip Patch Antenna using PIN Diodes. In *Proceedings of APMC 2012*, Kaohsiung, 2012.
5. Aoad A, Simsek M, Aydin Z. Design of a Reconfigurable 5-Fingers Shaped Microstrip Patch Antenna by Artificial Neural Networks. *Int J Adv Res Comput Sci Software Eng (IJARCSSE)* 2014; **4**(10):61–70.
6. Christodoulou CG, Tawk Y, Lane SA, Erwin SR. Reconfigurable Antennas for Wireless and Space Applications. *Proc IEEE* 2012; **100**(7):2250–2261.
7. Ismail M, Rahim M, Majid H. The Investigation of PIN Diode Switch on Reconfigurable Antenna. In *2011 IEEE International RF and Microwave Conference (RFM 2011)*, Seremban, Malaysia, 2011.
8. Khidre A, Lee KF, Yang F, Elsherbeni AZ. Circular Polarization Reconfigurable Wideband E-Shaped Patch Antenna for Wireless Applications. *IEEE Trans Antennas Propag* 2013; **61**(2):960–964.
9. Chen RH, Row JS. Single-Fed Microstrip Patch Antenna With Switchable Polarization. *IEEE Trans Antennas Propag* 2008; **56**(4):922–926.
10. Liu B, Aliakbarian H, Ma Z, Vandenbosch GAE, Gielen G, Excell P. An Efficient Method for Antenna Design Optimization Based on Evolutionary Computation and Machine Learning Techniques. *IEEE Trans Antennas Propag* 2014; **62**(1):7–18.
11. Ha BV, Zich RE, Pirinoli P, Hum SV. Application of Modified Bayesian Optimization Algorithm to the Design of Reflectarray Antenna. In *Numerical Electromagnetic Modeling and Optimization for RF, Microwave, and Terahertz Applications (NEMO)*, Pavia, Italy, 2014.
12. Chen G, Jiang H, Lei X. Reconfigurable Antenna Design Optimization Based on Improved Quantum Genetic Algorithm. In *General Assembly and Scientific Symposium (URSI GASS), IEEE CONFERENCE PUBLICATIONS*, 2014.
13. Zhu J, Bandler JW, Nikolova NK, Koziel S. Antenna Optimization Through Space Mapping. *IEEE Trans Antennas Propag* 2007; **55**(3):651–658.
14. Simsek M, Sengor NS. A Knowledge-Based Neuromodeling using Space Mapping Technique: Compound Space Mapping-Based Neuromodeling. *Inte J Numer Modell Electron Networks Devices Fields* 2008; **21**:133–149.
15. Patnaik A, Anagnostou D, Christodoulou CG, Lyke JC. Modeling Frequency reconfigurable Antenna Array Using Neural Networks. *Microwave Opt Technol Lett* 2005; **44**:351–354.
16. Khan T, De A. Design of Circular/Triangular Patch Microstrip Antennas using a Single Neural Model. In *Applied Electromagnetics Conference (AEMC), IEE*, Kolkata, India, 2011.
17. Simsek M, Tezel NS. The Reconstruction of Shape and Impedance Exploiting Space Mapping With Inverse Difference Method. *IEEE Trans Antennas Propag* 2012; **60**(4):1868–1877.
18. Zhang QJ, Gupta KC. *Neural Netwoks for RF and Microwave Design*. Artech House: Boston-London, 2000.
19. Simsek M, Zhang QJ, Kabir H, Sengor NS. The recent Developments in Microwave Design. *Int J Math Modell Numer Optim* 2011; **2**:213–228.
20. Krishna KR, Naryana JL, Reddy LP. A Neural Network Inverse Modeling Approach for the design of Spiral Inductor. *Int J Conf Comput Sci Eng Technol (IJCSET)* 2011; **2**(3):54–64.
21. Simsek M, Sengor NS. An efficient Inverse ANN Modeling Approach Using Prior Knowledge Input with Difference Method. In *European Conference on Circuit Theory and Design*, Antalya, 2009.
22. Kabir H, Wang Y, Yu M, Zhang Q-J. Neural Network Inverse Modeling and Applications to Microwave Filter Design. *IEEE Trans Microwave Theory Tech* 2008; **56**(4):867–879.
23. Watson PM, Gupta KC, Mahajan RL. Development of Knowledge Based Artificial Neural Network Models for Microwave Components, in *Microwave Symposium Digest*. IEEE MTT-S International: Baltimore, MD, USA 1998 9–12.
24. Constatine B. *Antenna Theory Analysis and Design*, vol. 3rd. John Wiley & Sons: New Jersey, Hoboken 2005.
25. Bernhard JT. *Reconfigurable Antennas*. Morgan & Claypool Publishers: Champaign, 2007.
26. Information and Telecommunication Technology Center (ITTC). [Online]. Available: http://www.ittc.ku.edu/. [Accessed 10 February 2015].
27. Wang F, Zhang QJ. Knowledge-Based Neural Models for Microwave Design. *IEEE Transaction on Microwave Theory and Techniques* 1997; **45**(12):2333–2343.
28. Watson P, Gupta K. EM-ANN Models for Microstrip Vias and interconnects in Dataset Circuits. *IEEE Trans Microwave Theory Tech* 1996; **44**(12):2495–2503.
29. Koziel S, Bekasiewicz A, Zieniutycz W. Expedited EM-Driven Multiobjective Antenna Design in Highly Dimensional Parameter Spaces. *IEEE Antennas Wirel Propag Lett* 2014; **13**:631–634.
30. Khan T, De A, Uddin M. Prediction of Slot-Size and Inserted Air-Gap for Improving the Performance of Rectangular Microstrip Antennas Using Artificial Neural Networks. *IEEE Antennas Wirel Propag Lett* 2013; **12**:1367–1371.
31. Neural Network Toolbox. [Online]. Available: http://www.mathworks.com/help/nnet/index.html. [Accessed 01 February 2015].

DOI: 10.1002/jnm